J. Fluid Mech. (1994), *vol.* 260, *pp.* 57–80

Topological vortex dynamics in axisymmetric viscous flows

By MOGENS V. MELANDER[1] AND FAZLE HUSSAIN[2]

[1] Department of Mathematics, Southern Methodist University, Dallas, TX 75275, USA

[2] Department of Mechanical Engineering, University of Houston, Houston, TX 77204, USA

(Received 23 March 1993 and in revised form 27 July 1993)

The topology of vortex lines and surfaces is examined in incompressible viscous axisymmetric flows with swirl. We argue that the evolving topology of the vorticity field must be examined in terms of axisymmetric vortex surfaces rather than lines, because only the surfaces enjoy structural stability. The meridional cross-sections of these surfaces are the orbits of a dynamical system with the azimuthal circulation being a Hamiltonian H and with time as a bifurcation parameter μ. The dependence of H on μ is governed by the Navier–Stokes equations; their numerical solutions provide H. The level curves of H establish a time history for the motion of vortex surfaces, so that the circulation they contain remains constant. Equivalently, there exists a *virtual velocity field* in which the motion of the vortex surfaces is frozen almost everywhere; the exceptions occur at critical points in the phase portrait where the virtual velocity is singular. The separatrices emerging from saddle points partition the phase portrait into *islands*; each island corresponds to a structurally stable vortex structure. By using the flux of the meridional vorticity field, we obtain a precise definition of reconnection: *the transfer of flux between islands*. Local analysis near critical points shows that the virtual velocity (because of its singular behaviour) performs 'cut-and-connect' of vortex surfaces with the correct rate of circulation transfer – thereby validating the long-standing viscous 'cut-and-connect' scenario which implicitly assumes that vortex surfaces (and vortex lines) can be followed over a short period of time in a viscous fluid. Bifurcations in the phase portrait represent (contrary to reconnection) changes in the topology of the vorticity field, where islands spontaneously appear or disappear. Often such topology changes are catastrophic, because islands emerge or perish with finite circulation. These and other phenomena are illustrated by direct numerical simulations of vortex rings at a Reynolds number of 800.

1. Introduction

Vortex reconnection is in many ways a controversial subject. In spite of numerous computational (e.g. Schwarz 1985; Ashurst & Meiron 1987; Kida & Takaoka 1991) and experimental (Fohl & Turner 1975; Schatzle 1987; Oshima & Izutzu 1988) investigations, the literature offers only conflicting suggestions for the physical mechanism and its characteristics. Moreover, the hydrodynamical significance of the phenomenon is still unclear. Is it one of the following: a prime candidate for a finite-time singularity in the Euler equations (e.g. Pumir & Siggia 1992; Kerr 1992; Caflisch, Li & Shelley 1993); instrumental in turbulence cascade (Melander & Hussain 1991); critical to coherent structure dynamics, mixing, aerodynamic noise generation (Hussain 1986); essential for the production of helicity (Hussain 1986); or could it be an inconsequential aspect of three-dimensional flows, whose relevant characteristics can

be obtained by other means? Even the nature of vortex reconnection is a matter of debate. Is it essentially a large-scale phenomenon, or intrinsically associated with the smallest scales? Is it viscous, essentially inviscid, or a combination of both? The different views are, perhaps, most clearly reflected in the various ways that the phenomenon has been simulated numerically: well-resolved direct numerical simulations (e.g. Kerr & Hussain 1989; Shelley, Meiron & Orszag 1993), vortex methods (e.g. Winkelmans & Leonard 1989), artificial viscosities (e.g. Zabusky & Melander 1989), etc. We are of the opinion that these controversies, in part, have their roots at a very basic question. Namely, can and should any importance be attached to vortex lines and surfaces in a viscous flow? These and other questions constitute the subject matter of *topological fluid mechanics*; see the proceedings of two recent conferences (Moffatt & Tsinober 1990; Moffatt *et al.* 1992). In an attempt to clarify some of the above controversies, or at least suggest an avenue by which this may be done, we consider viscous axisymmetric flows. Many aspects of topological vortex dynamics are revealed by axisymmetric flows. Their simplicity highlights topological problems and renders them manageable. These flows contain readily identifiable topological entities that are meaningful to track in time – a striking concept in viscous hydrodynamics. Axisymmetric viscous flows enable one to pinpoint surprising phenomena that would otherwise easily escape attention (even detection) in more complicated three-dimensional flows.

The axisymmetric geometry frees us from having to probe into three-dimensional flow fields via computer visualization and allows us to focus directly on the topology of the vorticity field. This analysis is greatly simplified by the existence of a family of axisymmetric vortex surfaces, which are easily obtained computationally. Mathematical tools to study their structure and evolution are readily available from the theory of dynamical systems and bifurcations. The entire mathematical framework is set up and adapted to topological vortex dynamics in §2.

In an inviscid incompressible fluid, all vortex lines are material; and in addition, the fluid velocity is circulation preserving (i.e. the circulation of any material vortex tube is constant in time). Vortex lines may still be material lines in a viscous fluid, but the fluid velocity is not circulation preserving; see Truesdell (1954). This fact, unfortunately, often leads to the prevalent view that vortex lines, surfaces, bundles, etc. cannot be tracked in time; and, therefore, have no physical relevance. This view is perhaps best expressed by Kida & Takaoka's (1991) footnote: 'The vortex lines are nothing but conceptual lines for convenience sake of visualising a vorticity field.' We disagree strongly with this view, for there may exist a *virtual* velocity (different from the material velocity) which is circulation preserving over most of the flow. Newcomb (1958) demonstrated that the motion of magnetic lines of force in a conducting plasma can, in general, be described by a virtual flux-preserving velocity field $\boldsymbol{v}_N$. Greene (1990) showed that Newcomb's results can be translated to the motion of vortex lines in a viscous incompressible fluid. This has important implications for the problem of vortex reconnection. The central idea is that if a circulation (i.e. flux)-preserving virtual velocity field $\boldsymbol{v}_N$ can be found, then we recover the inviscid vorticity theorems. Hence *a time-history can be assigned to the motion of vortex lines in a viscous flow*, for they are frozen in $\boldsymbol{v}_N$ *wherever it exists*. In axisymmetric flows, $\boldsymbol{v}_N$ does not exist in general (§4). However, another virtual velocity $\hat{\boldsymbol{v}}$, in which the axisymmetric vortex surfaces are frozen, does exist almost everywhere (§5). Moreover, $\hat{\boldsymbol{v}}$ is far easier to compute than $\boldsymbol{v}_N$ and identifies the structurally stable vortex line bundles, whose evolution can be followed. Also, $\hat{\boldsymbol{v}}$ correctly performs the 'cut and connect' (shown in figure 1) at points where it is singular (§6).

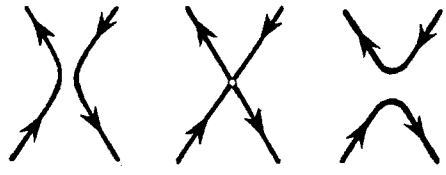

FIGURE 1. 'Cut-and-connect' schematic for two-dimensional vortex reconnection. Diffusion annihilates vorticity, whereby lines are cut and pasted together again as illustrated in the sequence $(a) \rightarrow (b) \rightarrow (c)$.

In spite of their simple geometry, axisymmetric flows exhibit interesting phenomena – even surprises (see §7). Among these are reconnections where vortex lines are parallel rather than anti-parallel, reconnections that reverse in time, vortex lines that change topology without reconnection, as well as the sudden appearance and disappearance of entire topological structures in the vorticity field. In more general three-dimensional flows, similar phenomena are expected to occur, but it will require extreme care to find them computationally; we show why.

Thus, viscous axisymmetric flows with swirl teach valuable lessons about topological vortex dynamics. The simple geometry allows a complete analysis in terms of well-developed mathematical tools. The relevant topological entities are easily identified and followed in time. Finally, these flows show how to proceed – as well as what to expect – in more complicated flows, where the computational, diagnostic and conceptual problems are much more difficult.

2. Dynamical systems approach

Consider a two-dimensional Hamiltonian system

$$\frac{\mathrm{d}x}{\mathrm{d}\sigma} = \frac{\partial H}{\partial y}, \quad \frac{\mathrm{d}y}{\mathrm{d}\sigma} = -\frac{\partial H}{\partial x}, \tag{1}$$

where σ is the independent variable, $H(x, y; \mu)$ is the Hamiltonian, and μ is a bifurcation parameter. Let H have the following two properties: H vanishes as x^2+y^2 tends to infinity, and H is a smooth function of x, y and μ.

For a particular value of μ, say μ_0, the phase portrait may appear as illustrated in figure 2(*a*). This sketch shows three critical points: two centres (A and C) and one saddle (B). From a topological standpoint, the set $\mathfrak{X}$ of all trajectories is naturally partitioned in the following way:

$$\mathfrak{X} = A \cup B \cup C \cup \mathfrak{S}_A \cup \mathfrak{S}_C \cup \mathfrak{I}_A \cup \mathfrak{I}_C \cup \mathfrak{I}_{ABC}. \tag{2}$$

Here A, B and C are the critical points; $\mathfrak{S}_A$ and $\mathfrak{S}_C$ are the separatrices emerging from B and enclosing centres A and C, respectively; $\mathfrak{I}_A$ is the set of closed trajectories enclosing A, but not C; $\mathfrak{I}_C$ contains the orbits surrounding only C; and $\mathfrak{I}_{ABC}$ holds the trajectories enclosing all three critical points. Following MHD terminology, $\mathfrak{I}_A$, $\mathfrak{I}_C$ and $\mathfrak{I}_{ABC}$ are called *islands* (e.g. Greene 1990).

A flux is associated with the vector field $(\mathrm{d}x/\mathrm{d}\sigma, \mathrm{d}y/\mathrm{d}\sigma)$. If $\mathscr{L}$ is an orientated curve connecting points P and Q in the (x, y)-plane, then the *flux* through $\mathscr{L}$ is

$$\Gamma_{PQ} = \int_P^Q \left(\frac{\mathrm{d}x}{\mathrm{d}\sigma} n_x + \frac{\mathrm{d}y}{\mathrm{d}\sigma} n_y\right) \mathrm{d}s, \tag{3}$$

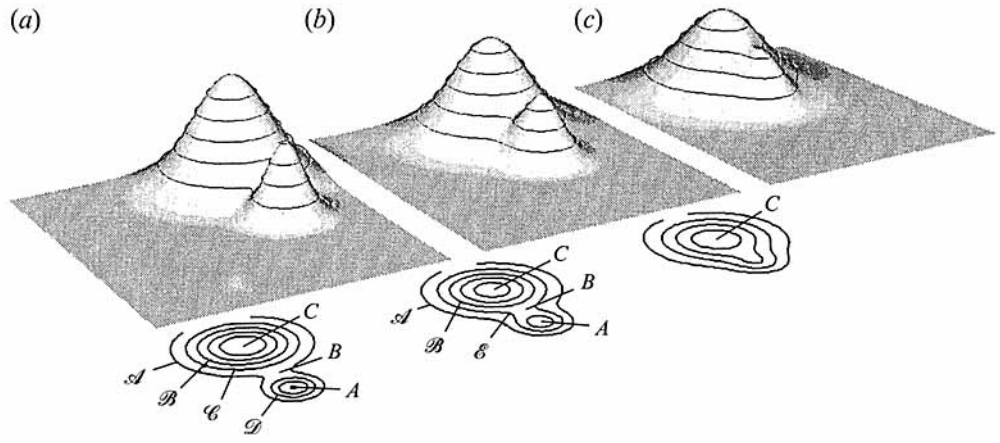

FIGURE 2. Carpet plots of the Hamiltonian H (top) and corresponding phase portraits (bottom) for three different values of the bifurcation parameter μ.

where $\boldsymbol{n} = (n_x, n_y)$ is the local unit vector normal to $\mathscr{L}$, and s is the arclength. It follows at once from (1) that $\Gamma_{PQ} = H(Q) - H(P)$. Each island $\mathfrak{I}$ has a flux, *the island flux* $\Gamma(\mathfrak{I})$, which we define as the flux of a curve $\mathscr{L}$ intersecting all trajectories in $\mathfrak{I}$ exactly once, the orientation of $\mathscr{L}$ being from the outside to the inside of the island. Hence, $\Gamma(\mathfrak{I})$ is positive when the orbits are clockwise. Relating this to figure 2(*a*), we have

$$\Gamma(\mathfrak{I}_A) = H(A) - H(B), \quad \Gamma(\mathfrak{I}_C) = H(C) - H(B)$$

and

$$\Gamma(\mathfrak{I}_{ABC}) = H(B) - H(\infty) = H(B).$$

Now consider the μ-dependence of (1). Here the smoothness of H is important, for it guarantees structural stability for almost all values of μ. The phase portrait in figure 2(*a*), for example, is structurally stable. Hence, the partitioning (2) is also valid when μ is in an open interval around μ_0. When μ is increased *slightly*, the critical points, separatrices, and islands may, however, shift slightly in the phase plane; consequently, the island fluxes may also change slightly. Island fluxes can change by (i) annihilation, (ii) creation, and (iii) transfer from neighbouring islands. In the context of figure 2(*a*), we have flux annihilation in $\mathfrak{I}_A$ if $H(A)$ decreases with μ; and flux creation, if $H(A)$ increases. Moreover, the islands $\mathfrak{I}_A$ and $\mathfrak{I}_C$ transfer flux to $\mathfrak{I}_{ABC}$ if $H(B)$ increases with μ. Thus, we *define reconnection as the exchange of flux between neighbouring islands in a structurally stable phase portrait*. Note that this is the definition commonly used in MHD (Greene 1988, 1990). The rate at which an island *gains* flux through reconnection is the *reconnection rate* R_{rec}.

The μ-dependence becomes particularly interesting when individual orbits are labelled and tracked as the phase portrait changes. The phase portrait inherits a natural labelling, because H is constant along trajectories for any given value of μ. Thus the 'μ-history' of individual trajectories is established by following fixed levels of H. Crucially, the flux contained between two trajectories is preserved. We must be aware, though, that orbits can appear, disappear, or reconnect with others. In fact, this is exactly what we wish to focus on. A structurally stable phase portrait (e.g. figure 2*a*) allows the following changes when μ is increase slightly.

(i) *Continuous deformation of a trajectory*. As an example consider the trajectories labelled $\mathscr{A}$ and $\mathscr{B}$ in figure 2(*a*, *b*). Here a small change in μ results in small deformations of $\mathscr{A}$ and $\mathscr{B}$.

(ii) *Creation of trajectories.* This happens when a local maximum of H increases (or a local minimum of H decreases).

(iii) *Annihilation of trajectories.* This occurs when a local minimum of H increases (or a local maximum of H decreases).

(iv) *Joining of two trajectories into one.* As an example consider the trajectories labelled $\mathscr{C}$ and $\mathscr{D}$ in figure 2(*a*). These trajectories are very close to the separatrices. A small increase in μ combines $\mathscr{C}$ and $\mathscr{D}$ into a single trajectory $\mathscr{E}$ (figure 2*b*) through a small change in $H(B)$.

(v) *Splitting of one trajectory into two.* This is event (iv) occurring in reverse.

The most likely occurrence is event (i) since it happens everywhere, except near critical points. Events (ii) and (iii) are more rare for they occur only at critical points of the centre type; these points are located well inside islands. Events (iv) and (v) are reconnections and represent precisely the discontinuous line evolution intuitively thought of as reconnection, i.e. cut-and-connect as illustrated in figure 1.

A drastic increase in μ can cause a bifurcation in the phase portrait, as indicated in figure 2(*b*, *c*). In this way, old islands are destroyed or new ones are generated, and thereby the topology of the vector field $(\mathrm{d}x/\mathrm{d}\sigma, \mathrm{d}y/\mathrm{d}\sigma)$ is altered. We call such an event a *spontaneous topological change*: 'spontaneous', because it occurs exactly when μ exceeds a critical value μ_{crit}, and 'topological', because the topology of the phase portrait is different for $\mu < \mu_{crit}$ and $\mu > \mu_{crit}$. If islands are created or destroyed with finite flux at $\mu = \mu_{crit}$, then we call the bifurcation a *catastrophic topology change.*

It is important to distinguish between reconnection and a spontaneous topological change; they are conceptually different phenomena. Reconnection relies on the flux concept, but a spontaneous topological change does not. Reconnection refers to topological changes in the *labelled orbits* of a structurally stable phase portrait and reflects a continuous transfer of flux between neighbouring islands. In particular, reconnection does not change the topology of the phase portrait. A spontaneous topology change, on the other hand, is a sudden change in the topology of the phase portrait, where entire islands are generated or destroyed.

Vortex reconnection follows precisely the above description in some flows. To see this, consider the Navier–Stokes equations with translational invariance in one direction (say the vertical direction z). That is, $v = (u(x,y), v(x,y), w(x,y))$; $p = p(x,y)$; $\omega = \nabla \times v = (\omega_x(x,y), \omega_y(x,y), \omega_z(x,y))$. Here we immediately find that

$$\omega_x = \frac{\partial w}{\partial y}, \quad \omega_y = -\frac{\partial w}{\partial x}, \tag{4}$$

where

$$\frac{\partial w}{\partial t} = -u\frac{\partial w}{\partial x} - v\frac{\partial w}{\partial y} + \nu\left(\frac{\partial^2 w}{\partial x^2} + \frac{\partial^2 w}{\partial y^2}\right), \tag{5}$$

$$\frac{\partial \omega_z}{\partial t} + u\frac{\partial \omega_z}{\partial x} + v\frac{\partial \omega_z}{\partial y} = \nu\left(\frac{\partial^2 \omega_z}{\partial x^2} + \frac{\partial^2 \omega_z}{\partial y^2}\right), \tag{6}$$

and u, v are determined entirely by ω_z, assuming that the flow vanishes as $x^2 + y^2$ tends to infinity. We observe that ω_z obeys the equations of two-dimensional vortex dynamics, because ω_x and ω_y have no effect on the evolution of ω_z. The dynamics of the in-plane vorticity follows from (4) and (5), the latter being a passive scalar transport equation. Note that the in-plane vorticity is subject to both vortex stretching and diffusion. Comparing with the Hamiltonian system (1), we see a perfect analogy. The phase plane is the (x,y)-plane, and trajectories of the dynamical system are vector lines of the in-plane vorticity field. The Hamiltonian H is the vertical velocity w; the flux is

circulation per unit length in vertical planes; and the bifurcation parameter μ is time t. Note, however, that the Hamiltonian w depends in a complicated manner on the bifurcation parameter t, namely through the diffusive scalar transport equation (5) with the velocity field determined by (6). Interestingly, this analogy between a fluid mechanical problem and a parameter-dependent dynamical system suggest how a time history of vortex lines in a viscous fluid can be established in a meaningful way.

3. Governing equations for axisymmetric flows

In axisymmetric geometry, the pressure, velocity, and vorticity depend only on r and z. Therefore, the governing equations for a viscous, constant-property, incompressible flow can be expressed in terms of three variables: ψ, η and ξ. Here ψ gives the meridional flow

$$v_r = \frac{1}{r}\frac{\partial \psi}{\partial z}, \quad v_z = -\frac{1}{r}\frac{\partial \psi}{\partial r}; \tag{7}$$

$\eta \equiv \omega_\theta / r = (1/r^2)\partial^2\psi/\partial r^2 - (1/r^3)\,\partial\psi/\partial r + (1/r^2)\,\partial^2\psi/\partial z^2$; and $\xi \equiv 2\pi r v_\theta = \text{constant}$ gives the axisymmetric vortex surfaces, because

$$\omega_r = -\frac{1}{2\pi r}\frac{\partial \xi}{\partial z}, \quad \omega_z = \frac{1}{2\pi r}\frac{\partial \xi}{\partial r}. \tag{8}$$

In terms of η and ξ, the governing equations are

$$\frac{\mathrm{D}\xi}{\mathrm{D}t} = \nu\left(\frac{\partial^2 \xi}{\partial r^2} - \frac{1}{r}\frac{\partial \xi}{\partial r} + \frac{\partial^2 \xi}{\partial z^2}\right), \tag{9}$$

$$\frac{\mathrm{D}\eta}{\mathrm{D}t} = \frac{1}{4\pi^2 r^4}\frac{\partial \xi^2}{\partial z} + \nu\left(\frac{\partial^2 \eta}{\partial r^2} + \frac{3}{r}\frac{\partial \eta}{\partial r} + \frac{\partial^2 \eta}{\partial z^2}\right), \tag{10}$$

with $\mathrm{D}/\mathrm{D}t \equiv \partial/\partial t + v_r\,\partial/\partial r + v_z\,\partial/\partial z$.

4. Why not study vortex line topology?

Consider the instantaneous vorticity field in an axisymmetric flow with swirl. An arbitrary vortex line $\mathscr{L}$ is confined to one connected ξ = constant surface. Because of axisymmetry, all vortex lines on this surface have exactly the same shape as $\mathscr{L}$; i.e. $\mathscr{L}$ can be made to coincide with any other vortex line on the surface by an appropriate rotation about the z-axis.

Each closed ξ-contour in the meridional plane is a cross-section of a toroidal vortex surface. Let $\mathscr{T}$ be one of these surfaces. All vortex lines on $\mathscr{T}$ obviously have exactly the same winding number W (W is defined as the number of times a vortex line coils around the minor toroidal axis for each time it circles the z-axis). In the neighbourhood of $\mathscr{T}$, the dependence of W on ξ is continuous. Thus, either W is constant across surfaces, or surfaces with rational and irrational winding numbers are spaced infinitely close together. On surfaces with rational W, the vortex lines close on themselves, while on surfaces with irrational W, they do not. In fact, a single line fills the entire surface in the latter case.

The implications are important, for in order to establish a 'time-history' of vortex lines in a viscous flow, there is only one meaningful way to proceed: to find a circulation-preserving velocity field $\boldsymbol{v}_N$ in which the vortex lines are frozen. This velocity is necessarily different from the material velocity; see Truesdell (1954, p. 86). Newcomb (1958) showed how such a virtual velocity can be found for the motion of

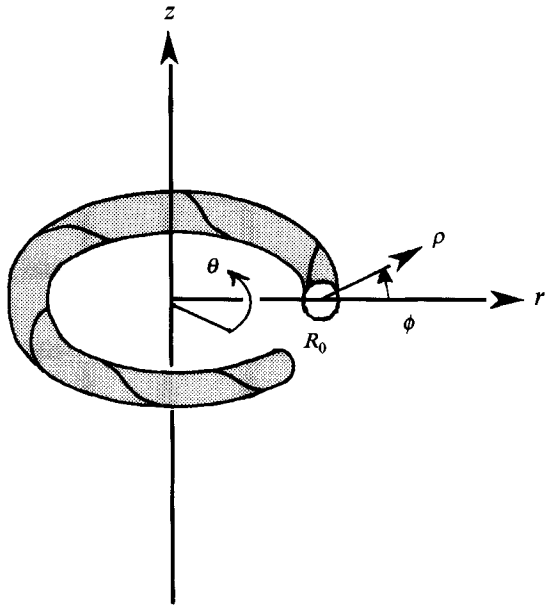

FIGURE 3. Schematic showing the local coordinate system (ρ, ϕ) in the meridional plane. An axisymmetric vortex surface and a vortex line with $W \approx 7$ are also shown.

magnetic lines of force in a conducting plasma. His analysis and results readily translate to the motion of vortex lines in a viscous fluid (Greene 1990). Under some circumstances, however, such a virtual velocity does not exist *everywhere* along a vortex line. One such case is when the vortex line closes on itself and, in addition, the line integral of $\nu\boldsymbol{\omega} \cdot \nabla \times \boldsymbol{\omega}$ does not vanish; see Greene (1990). For axisymmetric flows with swirl, our above analysis of W shows, that such vortex lines are, in general, dense inside a toroidal vortex surface $\mathscr{T}$. Hence our $\boldsymbol{v}_N$ does not exist inside $\mathscr{T}$. In this sense, there are too many closed vortex lines in axisymmetric flows.

This analysis shows, for example, that it is not possible to assign a time history to the vortex lines in a viscous axisymmetric vortex ring with swirl. To highlight this problem, by way of example, we consider a thin vortex ring with a very large ring radius R_0 in a highly viscous flow. In this limit, the convective terms vanish, as do the diffusive terms proportional to $1/r$ in (9) and (10). The governing equations for ω_θ and ξ thereby both reduce to the heat equation. A vortex ring with self-similar diffusion of ω_θ and ξ is then described by

$$\omega_\theta = \frac{\Gamma}{4\pi\nu(t+t_0)} \exp\left(-\frac{\rho^2}{4\nu(t+t_0)}\right), \tag{11}$$

$$\xi = 4\pi\nu t_0 \frac{N}{R_0} \omega_\theta, \tag{12}$$

where ρ is the radius in a local polar coordinate system (ρ, ϕ) in the meridional plane centred at the vortex core (figure 3), $-t_0$ is the virtual origin of the classical Stokes vortex (11), and N is an integer. The meridional vorticity is $\boldsymbol{\omega}_m = \omega_\phi \boldsymbol{e}_\phi = -(1/2\pi)(\partial\xi/\partial\rho)\boldsymbol{e}_\phi$; hence (12) yields

$$\omega_\phi = \frac{N\rho\omega_\theta}{R_0(1+t/t_0)}. \tag{13}$$

From (11) and (13), we obtain the winding number for a vortex line:

$$W = \frac{2\pi R_0/\omega_0}{2\pi\rho/\omega_\phi} = \frac{N}{1+t/t_0}. \tag{14}$$

This expression has two interesting aspects. First, all vortex lines have the same winding number; by construction $W = N$ at $t = 0$. Secondly, W decreases with time like $1/(t+t_0)$; thus, the vortex lines continuously change their topology. W is rational when t/t_0 is rational, and irrational otherwise. Therefore, the vortex lines are closed if and only if t/t_0 is rational. Note that the vortex lines constantly change their topology without any reconnection. Clearly, it cannot be meaningful to track such vortex lines (in their entirety) in time.

We conclude that nested toroidal vortex surfaces, with the same winding number for all vortex lines on each individual surface, constitute a structurally unstable vortex line configuration – even though the perturbations are restricted to be axisymmetric. As our interest is in coherent aspects of the vorticity field, we do not focus on the vortex line topology. Instead, we examine the topology of the axisymmetric vortex surface.

5. The virtual velocity field advecting axisymmetric vortex surfaces

The dynamics of axisymmetric flows with swirl follow precisely the dynamical system framework described in §2: ξ is the Hamiltonian H; the meridional plane (r, z) is the phase plane; t is the bifurcation parameter μ; flux is circulation of $\boldsymbol{\omega}_m \equiv (\omega_r, \omega_z)$; and islands are vortex structures consisting of nested axisymmetric vortex surfaces. This analogy with the dynamical system (1) shows that the level sets of ξ establish a time history of the axisymmetric vortex surfaces. In this section, we show that this time history allows us to introduce a virtual velocity field in which the motion of axisymmetric vortex surfaces is frozen.

Consider a material circle $\mathscr{C}$ in a plane normal to the z-axis and centred at $r = 0$. The circulation along $\mathscr{C}$ is given by

$$\Gamma_{\mathscr{C}} = \int_{\mathscr{C}} \boldsymbol{v} \cdot \mathrm{d}\boldsymbol{s} = 2\pi r_{\mathscr{C}} v_\theta = \xi, \tag{15}$$

where $r_{\mathscr{C}}$ is the radius of $\mathscr{C}$. Owing to axisymmetry, $\mathscr{C}$ remains circular as it moves with the material velocity $\boldsymbol{v}$. Thus, it readily follows from (9) that

$$\frac{\mathrm{d}\Gamma_{\mathscr{C}}}{\mathrm{d}t} = \frac{\mathrm{D}\xi}{\mathrm{D}t} = \frac{\partial\xi}{\partial t} + v_r\frac{\partial\xi}{\partial r} + v_z\frac{\partial\xi}{\partial z} = \nu\left(\frac{\partial^2\xi}{\partial r^2} - \frac{1}{r}\frac{\partial\xi}{\partial r} + \frac{\partial^2\xi}{\partial z^2}\right). \tag{16}$$

Now suppose that $\mathscr{C}$ is not material, but advected with some (axisymmetric) virtual velocity $\hat{\boldsymbol{v}} = (\hat{v}_r, \hat{v}_\theta, \hat{v}_z)$. In that case, the circulation of $\mathscr{C}$ changes at the rate

$$\begin{aligned}\left.\frac{\mathrm{d}\Gamma_{\mathscr{C}}}{\mathrm{d}t}\right|_{\hat{v}} &= \frac{\partial\xi}{\partial t} + \hat{v}_r\frac{\partial\xi}{\partial r} + \hat{v}_z\frac{\partial\xi}{\partial z} \\ &= \frac{\partial\xi}{\partial t} + v_r\frac{\partial\xi}{\partial r} + v_z\frac{\partial\xi}{\partial z} + (\hat{v}_r - v_r)\frac{\partial\xi}{\partial r} + (\hat{v}_z - v_z)\frac{\partial\xi}{\partial z} \\ &= \nu\left(\frac{\partial^2\xi}{\partial r^2} - \frac{1}{r}\frac{\partial\xi}{\partial r} + \frac{\partial^2\xi}{\partial z^2}\right) + \left((\hat{v}_r - v_r)\frac{\partial\xi}{\partial r} + (\hat{v}_z - v_z)\frac{\partial\xi}{\partial z}\right).\end{aligned} \tag{17}$$

In the last line, the first term is the effect of viscosity; the second is the effect of 'slip', i.e. the difference between virtual and material velocities. If these two effects balance, then the axisymmetric vortex surfaces are frozen in the virtual velocity field. Hence, we seek a $\hat{\boldsymbol{v}}$ such that

$$(\hat{v}_r - v_r)\frac{\partial \xi}{\partial r} + (\hat{v}_z - v_z)\frac{\partial \xi}{\partial z} = -\nu\left(\frac{\partial^2 \xi}{\partial r^2} - \frac{1}{r}\frac{\partial \xi}{\partial r} + \frac{\partial^2 \xi}{\partial z^2}\right). \tag{18}$$

Clearly, a velocity parallel to the axisymmetric vortex surfaces does not change $\Gamma_{\mathscr{C}}$. Therefore, we impose the extra condition that $\hat{\boldsymbol{v}} - \boldsymbol{v}$ must be perpendicular to these surfaces, i.e.

$$(\hat{v}_r - v_r)\frac{\partial \xi}{\partial z} - (\hat{v}_z - v_z)\frac{\partial \xi}{\partial r} = 0. \tag{19}$$

Equations (18) and (19) then determine the meridional component of $\hat{\boldsymbol{v}} - \boldsymbol{v}$. This system of equations has a unique solution if and only if the determinant $(\partial\xi/\partial r)^2 + (\partial\xi/\partial z)^2 = 4\pi^2 r^2(\omega_r^2 + \omega_z^2)$ is non-zero. In that case, we have

$$\begin{pmatrix} \hat{v}_r \\ \hat{v}_z \end{pmatrix} = \begin{pmatrix} v_r \\ v_z \end{pmatrix} - \nu \frac{(\partial^2\xi/\partial r^2) - (1/r)(\partial\xi/\partial r) + (\partial^2\xi/\partial z^2)}{(\partial\xi/\partial r)^2 + (\partial\xi/\partial z)^2} \begin{pmatrix} \partial\xi/\partial r \\ \partial\xi/\partial z \end{pmatrix}. \tag{20}$$

Obviously, the azimuthal component is of no consequence; for simplicity, let $\hat{v}_\theta = v_\theta$.

The determinant is zero at the points of vanishing meridional vorticity. There the system (18), (19) either has no solutions or infinitely many solutions: no solutions when $(\partial^2\xi/\partial r^2) - (1/r)(\partial\xi/\partial r) + (\partial^2\xi/\partial z^2 \neq 0$; infinitely many when $(\partial^2\xi/\partial r^2) - (1/r)(\partial\xi/\partial r) + (\partial^2\xi/\partial z^2) = 0$. In the latter case, any $(\hat{v}_r, \hat{v}_z)$ is a solution as every term in this system vanishes identically.

Thus, corresponding to the motion of ξ level curves, there is a virtual velocity field. It exists almost everywhere, and the axisymmetric surfaces are frozen in it. Specifically, $\hat{\boldsymbol{v}}$ exists where $\boldsymbol{\omega}_m$ is non-vanishing. There are, consequently, no topological changes in surfaces on which $|\boldsymbol{\omega}_m| \neq 0$. Note that although the material velocity field is divergence free, the virtual velocity is not. Moreover, the virtual velocity is the material velocity plus a correction, the slip, which is small away from critical points. The slip is directed such that ξ is always annihilated at centres (see (20)). Hence, creation of ξ is not possible.

6. Local analysis near typical nulls of the meridional vorticity

There are important reasons for analysing the behaviour of the virtual velocity near an $\boldsymbol{\omega}_m$ null. Such a null is a critical point in the dynamical system (1). It is here that islands can change circulation (flux) through annihilation and reconnection. By examining the singular behaviour of the virtual velocity near a null, we demonstrate through appropriate limiting processes that the virtual velocity produces the correct rate of annihilation and reconnection, namely those rates already known from the dynamical system discussion in §2. This is particularly interesting because the virtual velocity must perform the cut-and-connect procedure shown in figure 1.

For the Taylor expansion of ξ about a null (r_0, z_0) of the meridional vorticity field (ω_r, ω_z),

$$\xi = \xi_0 + \frac{1}{2}\left((r-r_0)^2 \frac{\partial^2\xi}{\partial r^2}\bigg|_0 + 2(r-r_0)(z-z_0)\frac{\partial^2\xi}{\partial r\,\partial z}\bigg|_0 + (z-z_0)^2\frac{\partial^2\xi}{\partial z^2}\bigg|_0\right) + \ldots, \tag{21}$$

we simplify the notation by

$$a \equiv \frac{\partial^2 \xi}{2\partial r^2}\bigg|_0, \quad b \equiv \frac{\partial^2 \xi}{2\partial r\,\partial z}\bigg|_0, \quad c \equiv \frac{\partial^2 \xi}{2\partial z^2}\bigg|_0, \quad \delta r \equiv r - r_0, \quad \delta z \equiv z - z_0.$$

Hence, $\xi - \xi_0$ is given locally by the quadratic form $a(\delta r)^2 + 2b\delta r\delta z + c(\delta z)^2$. The corresponding symmetric matrix is

$$\boldsymbol{M} = \begin{bmatrix} a & b \\ b & c \end{bmatrix}. \tag{22}$$

We let $(\delta r, \delta z) = (\rho\cos\phi, \rho\sin\phi)$, so as to pinpoint the singular part of $\hat{v}$. From (20) we obtain

$$\hat{\boldsymbol{v}}(\rho,\phi) = \frac{-\nu(a+c)}{\rho((a^2+b^2)\cos^2\phi + b(a+c)\sin 2\phi + (c^2+b^2)\sin^2\phi)} \boldsymbol{M}\begin{pmatrix}\cos\phi \\ \sin\phi\end{pmatrix} + O(1). \tag{23}$$

Clearly, the virtual velocity is singular at (r_0, z_0) if and only if $a+c \neq 0$. In that case, the singularity is $1/\rho$; this is the most singular that the virtual velocity can become at any null of ω_m.

Now that the order of the singularity is known, (23) can be simplified by introducing different local coordinates so that $\boldsymbol{M}$ becomes diagonal. Note that $\boldsymbol{M}$ is symmetric and thus has real eigenvalues (λ_1 and λ_2) and orthogonal eigenvectors ($\boldsymbol{e}_1$ and $\boldsymbol{e}_2$). If $b = 0$, the matrix is already diagonal. If $b \neq 0$, we have

$$\lambda_1 = \frac{a+c+((a-c)^2+4b^2)^{\frac{1}{2}}}{2}, \quad \lambda_2 = \frac{a+c-((a-c)^2+4b^2)^{\frac{1}{2}}}{2}, \tag{24}$$

and

$$\boldsymbol{e}_1 = \left[b, \frac{c-a}{2} + \left(\left(\frac{a-c}{2}\right)^2 + b^2\right)^{\frac{1}{2}}\right], \quad \boldsymbol{e}_2 = \left[\frac{c-a}{2} + \left(\left(\frac{a-c}{2}\right)^2 + b^2\right)^{\frac{1}{2}}, -b\right]. \tag{25}$$

Let the corresponding unit eigenvectors be $\hat{\boldsymbol{e}}_1$ and $\hat{\boldsymbol{e}}_2$. Using these vectors as basis vectors in a new local coordinate system (χ_1, χ_2), the quadratic form (21) becomes

$$\xi(\chi_1, \chi_2) = \xi_0 + \lambda_1\chi_1^2 + \lambda_2\chi_2^2. \tag{26}$$

In these coordinates the singular part of virtual velocity field (23) is

$$\hat{\boldsymbol{v}} = \begin{pmatrix}\hat{v}_1 \\ \hat{v}_2\end{pmatrix} = \frac{-\nu(\lambda_1+\lambda_2)}{\lambda_1^2\chi_1^2 + \lambda_2^2\chi_2^2}\begin{pmatrix}\lambda_1\chi_1 \\ \lambda_2\chi_2\end{pmatrix}. \tag{27}$$

When the eigenvalues have the same sign, the critical point is a centre for the meridional vorticity and a sink of nodal form for the virtual velocity (see (27) and figure 4*a*). At such a point, circulation of the meridional vorticity field is annihilated. The rate of annihilation R_a (positive by definition) is determined by the singular part of the virtual velocity and the local quadratic form of ξ. We have

$$R_a = \lim_{\|(\chi_1,\chi_2)\|\to 0}\left|\frac{\xi(\chi_1,\chi_2) - \xi_0}{T(\chi_1,\chi_2)}\right|, \tag{28}$$

where $T(\chi_1, \chi_2)$ represents the time required for the virtual velocity field to carry an

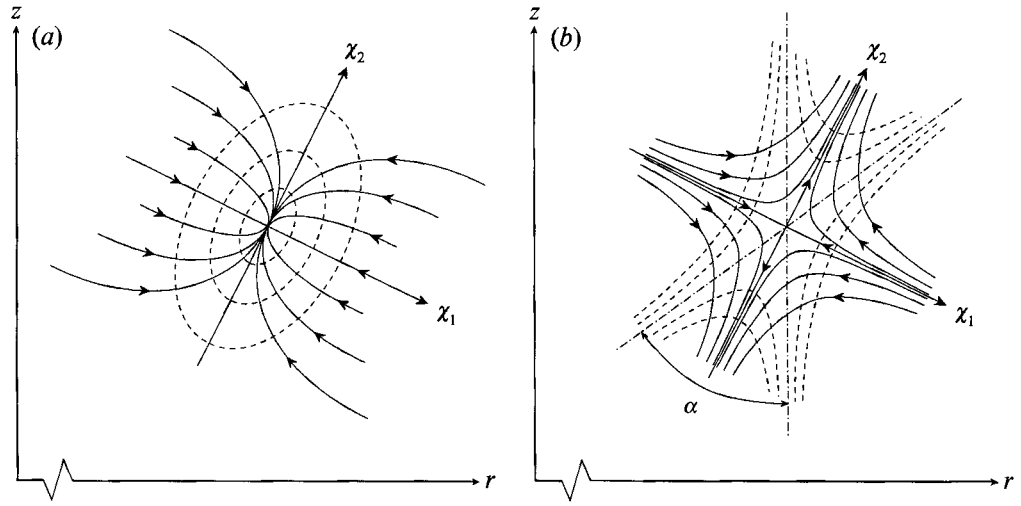

FIGURE 4. ξ-contours (---) and streamlines (——) of the slip $\hat{v}-v$ are sketched near typical isolated nulls of the meridional vorticity field ω_m: (*a*) a centre for the ξ-contours is a nodal sink for the slip; (*b*) a saddle for the ξ-contours is also saddle for the slip, but the separatrices are different. Also shown is the angle α between the ξ-separatrices.

object from location (χ_1, χ_2) to $(0,0)$. All points on a given ξ-contour have the same value of T. Therefore, T is most easily found by considering an object moving along one of the coordinate axes, say, the χ_1-axis. Thus,

$$T(\chi_1, 0) = \int_{\chi_1}^{0} \frac{\mathrm{d}x}{\hat{v}_1(x)} = (2\nu(1+\lambda_2/\lambda_1))^{-1}\chi_1^2; \tag{29}$$

substitution into (28) yields

$$R_a = 2\nu|(1+\lambda_2/\lambda_1)\lambda_1| = 2\nu|\lambda_1+\lambda_2| = 2\nu|a+c|. \tag{30}$$

When the eigenvalues have opposite signs the critical point is a saddle for both the meridional vorticity and the virtual velocity (see figure 4*b*). Here the ξ-contours are split and rejoined as they approach the critical point, exactly as suggested by the intuitive cut-and-connect cartoon (figure 1). By considering the motion of an object along one of the axes, we find the rate of circulation transfer

$$R_{rec} = \lim_{\|(\chi_1,\chi_2)\|\to 0} \left|\frac{\xi(\chi_1,\chi_2)-\xi_0}{T(\chi_1,\chi_2)}\right| = 2\nu|\lambda_1+\lambda_2| = 2\nu|a+c|. \tag{31}$$

Note that R_{rec} is positive by definition.

The virtual velocity results in exactly the same rates for change of circulation (flux) as the dynamical system approach in §2, because annihilation, as well as reconnection, occurs at the rate $2\nu|a+c|$, and

$$2\nu(a+c) = \nu\left(\frac{\partial^2\xi}{\partial r^2}+\frac{\partial^2\xi}{\partial z^2}\right)\bigg|_0 = \nu\left(\frac{\partial^2\xi}{\partial r^2}-\frac{1}{r}\frac{\partial\xi}{\partial r}+\frac{\partial^2\xi}{\partial z^2}\right)\bigg|_0 = \frac{\partial\xi}{\partial t}\bigg|_0 = \left(2\pi\nu r\left(\frac{\partial\omega_z}{\partial r}-\frac{\partial\omega_r}{\partial z}\right)\bigg|_0\right). \tag{32}$$

Here we have used $\partial\xi/\partial r|_0 = \partial\xi/\partial z|_0 = 0$, and $|_0$ indicates evaluation at the critical point.

For a saddle, the separatrices are locally the solutions to $\lambda_1 \chi_1^2 = -\lambda_2 \chi_2^2$. Thus, one of the angles between the separatrices is $\alpha = 2\arctan(-\lambda_2/\lambda_1)^{\frac{1}{2}}$, whereby (27) yields the following expression for the velocities along the coordinate directions:

$$\hat{v}_1(\chi_1, 0) = \nu \frac{\tan^2(\alpha/2) - 1}{\chi_1}, \quad \hat{v}_2(0, \chi_2) = \nu \frac{\cot^2(\alpha/2) - 1}{\chi_2}. \tag{33}$$

On the basis of (33), we conclude that the virtual flow, and hence the circulation transfer, is always from the wide-angle to the narrow-angle sector of the saddle; see figure 4(*b*). In the special case $\alpha = \pi/2$, there is no transfer and hence no reconnection.

Often the narrow angle between the separatrices at a saddle point is very small, because the gradient of ξ in one principal direction (say the χ_1-direction) is much larger than that in the other (i.e. $|\lambda_1/\lambda_2| \gg 1$). The circulation transfer is then from the χ_1-direction to the χ_2-direction as shown in figure 4(*b*). At a small distance ρ from the saddle point, the slip velocities along the two principal directions are very different in magnitude; (33) allows us to express their ratio in terms of the narrow angle α:

$$\frac{|\hat{\boldsymbol{v}}(0, \rho)|}{|\hat{\boldsymbol{v}}(\rho, 0)|} = \left| \frac{1 + \lambda_1/\lambda_2}{1 + \lambda_2/\lambda_1} \right| \approx |\lambda_1/\lambda_2| = \frac{1}{(\tan\frac{1}{2}\alpha)^2} \approx \frac{4}{\alpha^2} \gg 1. \tag{34}$$

Thus, when α is small, ξ-contours depart from the saddle point much faster than they approach it.

7. Analysis of numerical simulations

We illustrate the theoretical framework outlined above by direct numerical simulations of the Navier–Stokes equations. In particular, we wish to demonstrate, beyond any doubt, the occurrence of vortex reconnection, as well as the creation and destruction of structurally stable topological structures (islands). In addition, we wish to emphasize that these phenomena can be followed in complete detail by computational means, using the analytical framework discussed above. The numerical method used for the simulations is an axisymmetric spectral algorithm with eigenfunctions of the curl operator as basis functions; for details see Virk, Melander & Hussain (1994). We discuss four different cases. In the first two, the initial conditions have been chosen so as to force annihilation and creation of a saddle–centre pair. This we accomplish by having the azimuthal vorticity dominate the dynamics. Hence, it is not our intention that these two simulations should represent a realistic flow. The third simulation, however, represents a realistic flow, namely the evolution of a vortex ring with swirl. This flow was not specifically designed to produce reconnection. The fourth simulation features an additional symmetry, which allows us to comment on the vortex line topology: a surprising line topology evolves from a very simple one. Contrary to the first two simulations, the interaction between meridional and azimuthal vorticity is very strong here. The specific initial conditions for all simulations are given in the Appendix.

Case I: centre–saddle annihilation. It is well known that two vortex rings without swirl can leap-frog. Moreover, if the separation is smaller than a critical value, the two rings pair. Intuitively, such pairing should also occur in the presence of weak swirl; in this case, ξ is essentially a passive scalar. We selected the initial ω_θ as two rings that pair in the absence of swirl. ξ is chosen to be initially weak, and it has two peaks coinciding with the initial ω_θ peaks. Thereby we anticipate the two ξ-peaks will merge into one

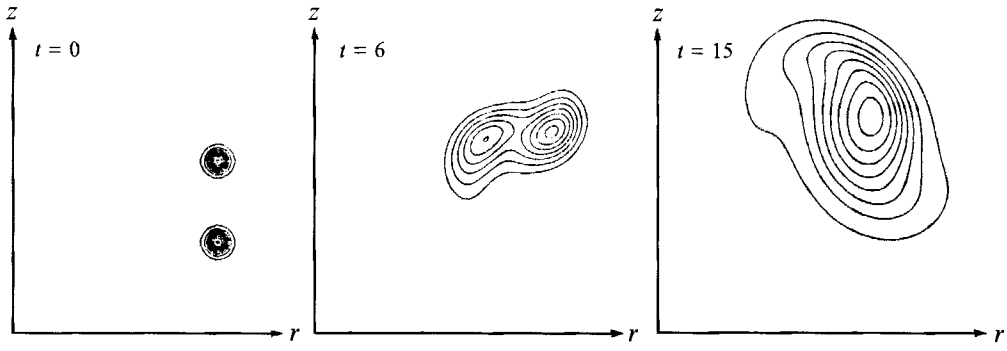

FIGURE 5. Evolution of ω_θ for case I.

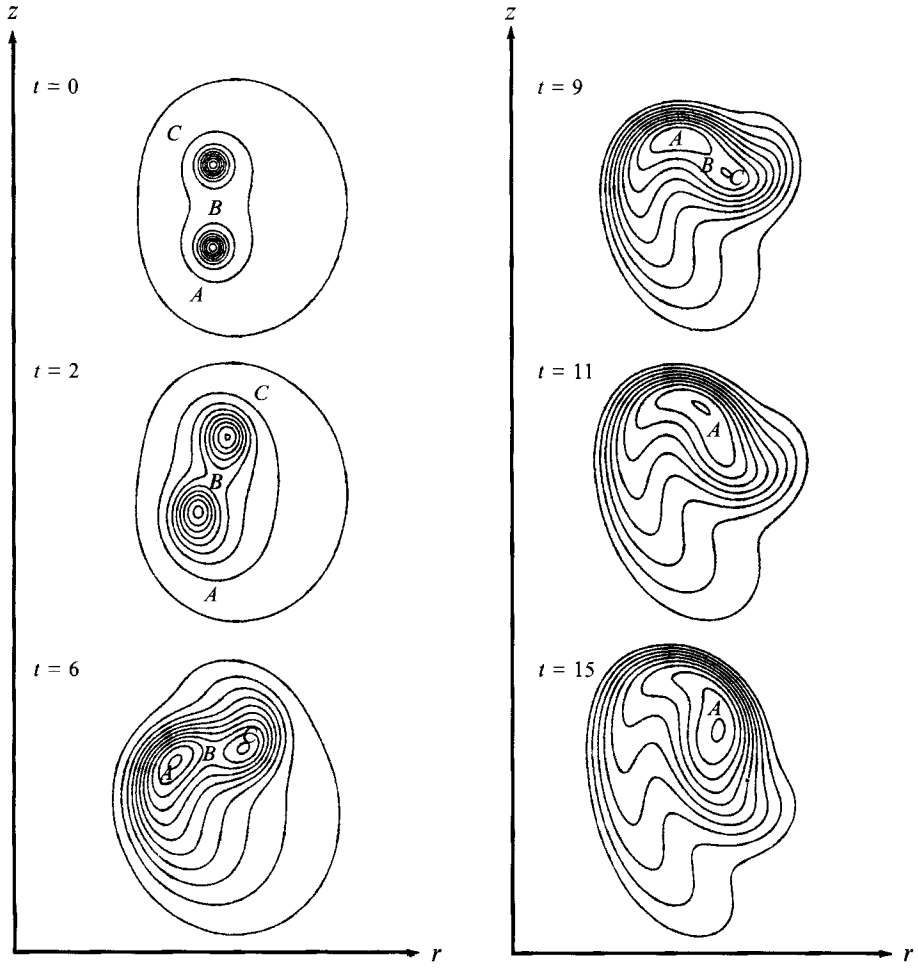

FIGURE 6. Evolution of the ξ-contours for case I.

during the pairing of the rings. Figures 5 and 6 show that the desired effect was indeed achieved. The initial trajectories ω_m (figure 6) feature exactly the same topology as in figure 2(*a*): namely one saddle (*B*), two centres (*A* and *C*), and three structurally stable islands ($\mathfrak{I}_A$, $\mathfrak{I}_B$ and $\mathfrak{I}_{ABC}$). Initially the saddle has no vorticity, because ω_θ is initially

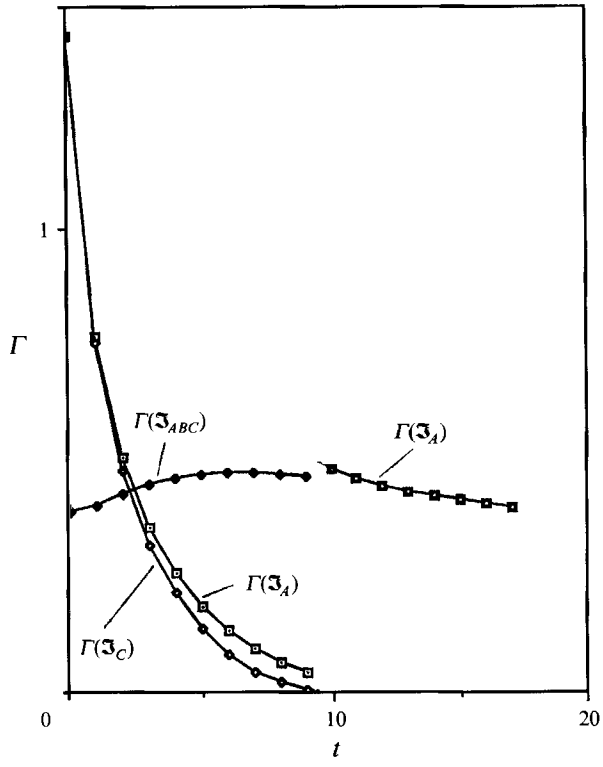

FIGURE 7. Evolution of the island circulations for case I. Note the discontinuous behaviour of $\Gamma(\mathfrak{J}_A)$ at $t = t_{crit} \approx 9.5$.

zero there. Hence, B does not initially correspond to a circular vortex line of the full three-dimensional vorticity field. However, B at once acquires azimuthal vorticity through diffusion. For $t > 0$, the saddle is, therefore, a point on a circular vortex line.

The three islands are present until a bifurcation of the phase portrait occurs at $t = t_{crit} \approx 9$ (see figure 7). Prior to this bifurcation, $\Gamma(\mathfrak{J}_A)$ and $\Gamma(\mathfrak{J}_C)$ change by two different processes: annihilation at A and C, and reconnection at B. It follows from our local analysis in §6 that the rates of circulation transfer from $\mathfrak{J}_A$ and $\mathfrak{J}_C$ to $\mathfrak{J}_{ABC}$ are equal. Moreover, $\Gamma(\mathfrak{J}_{ABC})$ changes by only one process, namely reconnection at B, as $\mathfrak{J}_{ABC}$ has no centres in its interior. Thus, we conclude:

(i) the circulation acquired by $\mathfrak{J}_{ABC}$ through reconnection equals $\xi_B(t) - \xi_B(0)$;
(ii) the circulation lost by $\mathfrak{J}_A$ (or $\mathfrak{J}_C$) through reconnection equals $\xi_B(t) - \xi_B(0)$;
(iii) the circulation lost by $\mathfrak{J}_A$ through annihilation at A equals $\xi_A(0) + \xi_B(0) - \xi_A(t) - \xi_B(t)$;
(iv) the circulation lost by $\mathfrak{J}_C$ through annihilation at C equals $\xi_C(0) + \xi_B(0) - \xi_C(t) - \xi_B(t)$.

The circulation of each island is easily obtained from ξ: $\Gamma(\mathfrak{J}_A) = \xi_A - \xi_B$, $\Gamma(\mathfrak{J}_C) = \xi_C - \xi_B$, and $\Gamma(\mathfrak{J}_{ABC}) = \xi_B$. Figure 7 shows the circulation of each island during the evolution. Immediately from the beginning, there is reconnection of axisymmetric vortex surfaces at B, and circulation is transferred from $\mathfrak{J}_A$ and $\mathfrak{J}_B$ to $\mathfrak{J}_{ABC}$. Around $t = 7$ this transfer gradually comes to a halt, and the reconnection reverses, so that circulation is transferred from $\mathfrak{J}_{ABC}$ rather than to $\mathfrak{J}_{ABC}$. This reversal occurs because the angle α between the separatrices at B increases through $\pi/2$, whereby the virtual

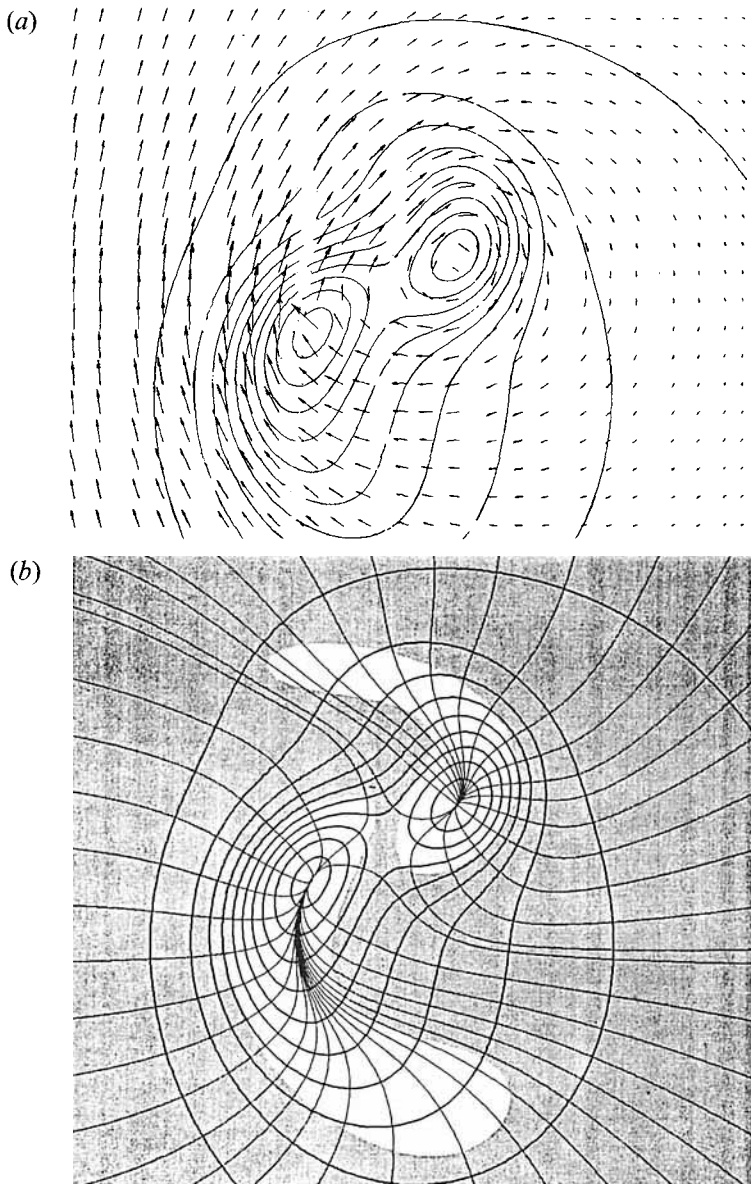

FIGURE 8. (*a*) Vector plot of the virtual velocity field at $t = 5$. (*b*) Corresponding streamlines of the slip $(\hat{v}-v)$. Within the shaded region the slip is directed away from the nodal points; in the white region, toward the nodal points. Contours of ξ are overlaid in both figures.

velocity reverses its direction near B (see (33)). Meanwhile, circulation of $\mathfrak{I}_A$ and $\mathfrak{I}_B$ is annihilated rather quickly at A and B.

The axisymmetric vortex surfaces are frozen in the virtual velocity field except at critical points. While the slip velocity is unbounded at the critical points, it is rather small everywhere else. Consequently, the virtual velocity looks like the material velocity in most of the flow region; figure 8(*a*) shows the virtual velocity field at $t = 5$. The slip velocity (figure 8*b*) is more informative regarding annihilation and reconnection than the virtual velocity. Figure 8(*b*) has several interesting features. We observe that the slip velocity has nodal points at A and C and one saddle at B.

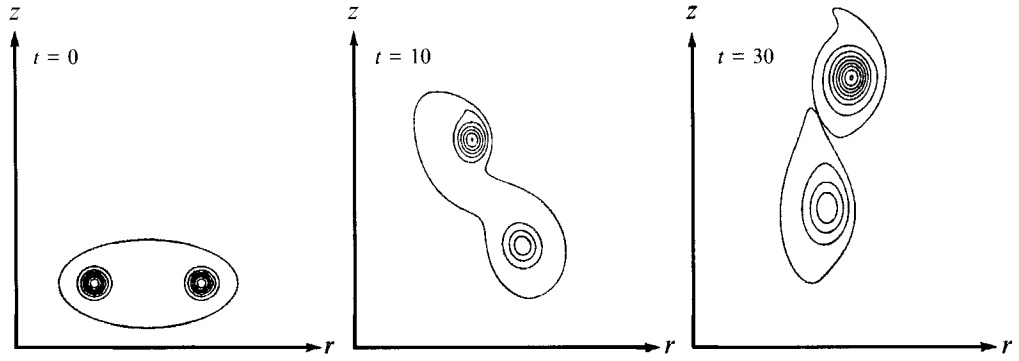

FIGURE 9. Evolution of ω_θ for case II.

Moreover, the direction of slip is toward the singular nodes in some areas (the white regions in figure 8*b*) and away from nodes in other areas (the shaded regions in figure 8*b*). Thus, inside the white regions, the ξ-contours contract towards the nodal points; the ξ-contours expand in the shaded region. As the flow evolves, the white regions become larger, merge into one, and eventually engulf the saddle point B, so as to reverse the circulation transfer at B.

The bifurcation at $t = t_{crit}$ is a centre–saddle annihilation. Afterwards, only one island remains. This topological change from three islands to one is clearly evident in figure 6. We observe that the island $\mathfrak{I}_C$ diminishes in size much quicker than $\mathfrak{I}_A$. More precisely, $\Gamma(\mathfrak{I}_C)$ decays faster than $\Gamma(\mathfrak{I}_A)$; see figure 7. At $t = t_{crit}$, $\Gamma(\mathfrak{I}_C)$ vanishes, while $\Gamma(\mathfrak{I}_A)$ is still finite. Hence, there is a catastrophic change in the topology at $t = t_{crit}$. Specifically, $\mathfrak{I}_A$ merges with $\mathfrak{I}_{ABC}$ as the separatrices dividing these islands disappear along with B. The surviving island is then $\mathfrak{I}_A$, which was spontaneously extended to the entire meridional plane. Consequently, reconnection at B terminates exactly at $t = t_{crit}$, and there is a discontinuity in $\Gamma(\mathfrak{I}_A)$; see figure 7. The bifurcation also affects the virtual velocity field $\hat{\boldsymbol{v}}$, for as C and B disappear, $\hat{\boldsymbol{v}}$ loses two singularities (see (20)). As the bifurcation takes place, two circular vortex lines (corresponding to B and C) of the full three-dimensional vorticity field spontaneously disappear. Note that this disappearance is not due to the cancellation of anti-parallel vorticity, for the two vortex lines both have positive ω_θ.

Case II: centre–saddle creation. Our initial condition, once again, consists of two vortex rings with weak swirl. This time we do not want the rings to pair. Instead we use the strain-rate field between two corotating rings to split a single ξ-peak into two. The simulation, shown in figure 9 and 10, accomplishes just that.

Two bifurcations have occurred prior to $t = 18$; see figure 10. The first creates a centre (C) and a saddle (B). $\Gamma(\mathfrak{I}_A)$ remains continuous during this bifurcation, because the new critical points emerge exactly at A. Hence, this topological change is not catastrophic. The second bifurcation creates a new saddle (D) and a new centre (E) above A; see frame $t = 18$. This saddle–centre pair emerges some distance away from A, although still inside the separatrix $\mathfrak{S}_A$. Thereby $\mathfrak{I}_A$ splits up into three islands: $\mathfrak{I}_A$ (now bounded by a separatrix emerging from D), $\mathfrak{I}_E$, and $\mathfrak{I}_{ADE}$. As a result of this bifurcation, $\Gamma(\mathfrak{I}_A)$ decreases spontaneously by a finite amount, which then becomes $\Gamma(\mathfrak{I}_{ADE})$. Hence, the second bifurcation is a catastrophic change of topology, i.e. a new island is born with finite circulation.

$\Gamma(\mathfrak{I}_E)$ is zero when the island is created by the second bifurcation. It then increases, reaches a maximum, and starts decreasing. By $t = 30$, E and D have disappeared again,

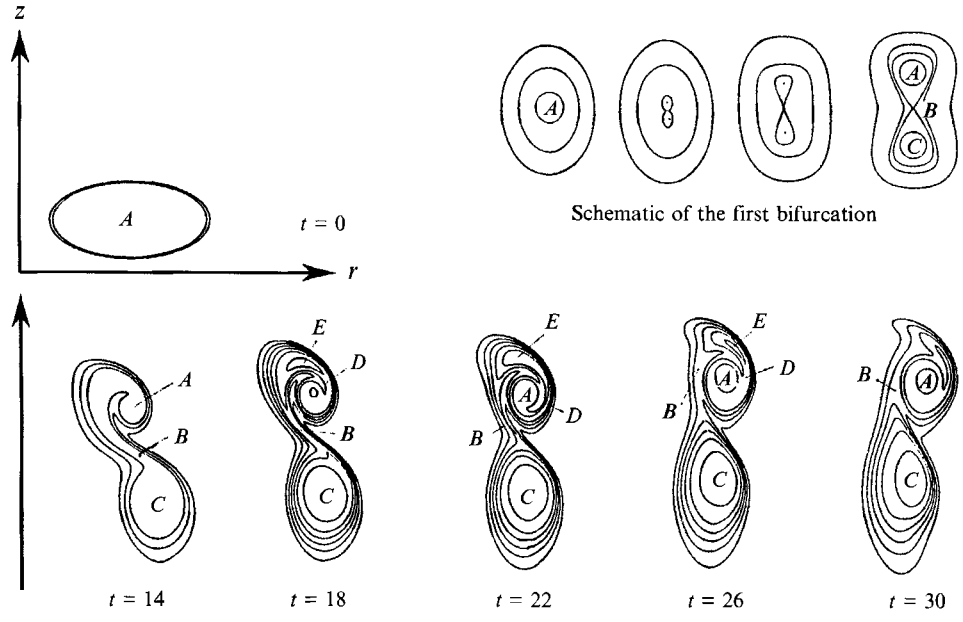

FIGURE 10. Evolution of the ξ-contours for case II. Also shown is a schematic of the first bifurcation.

indicating that a third bifurcation has taken place between $t = 26$ and 30 (figure 10). At the time of bifurcation, $\Gamma(\mathfrak{I}_E)$ vanishes, but $\Gamma(\mathfrak{I}_{ADE})$ is still finite. Since $\mathfrak{I}_{ADE}$ disappears with finite circulation, the third bifurcation is also a catastrophic topology change.

Case III: centre–saddle creation in a ring with swirl. Reconnection and topological changes in the vorticity field also occur in realistic axisymmetric flows. As an example, we mention the evolution of an axisymmetric 'partially polarized' vortex ring. The particular flow simulation used is case D in Virk *et al.* (1994); it is discussed in detail in that paper for other reasons. For our purposes, it suffices to say that the ring has significant swirl, i.e. ξ is not small and plays an active dynamical role. The initial ξ-distribution (figure 11 *a*) is a single-island configuration. During the evolution, the ring sheds a tail, and a bifurcation occurs to a three-island configuration, qualitatively similar to that in figure 2(*a*). Figure 11(*b*) shows the ξ-distribution at a late stage in the evolution, and figure 11(*c*) shows the corresponding vorticity magnitude $|\omega|$. Note that (34) applies to this surface reconnection, for the angle α between the separatrices at the saddle point is very narrow.

Comparison of figures 11(*b*) and 11(*c*) leads one to chilling reflections: a total failure of traditional diagnostic techniques. The vortical structure appears vastly different in these two figures. In fact, the only common features is the leading vortex ring, called the head. Judging just on the basis of figure 11(*c*), one would say that there are either one or two vortex structures, depending on whether the tail is regarded as connected or separated from the head. That there are, in fact three structures (islands) would escape detection, as would their location and extent. Moreover, the location of vortex reconnection would be totally misjudged (that is, if one even suspected the occurrence of reconnection). This shows that we need to be expressly cautious while analysing visualizations of fully three-dimensional vortex structures in terms of surfaces of constant vorticity magnitude. Note that surfaces of constant vorticity magnitude are

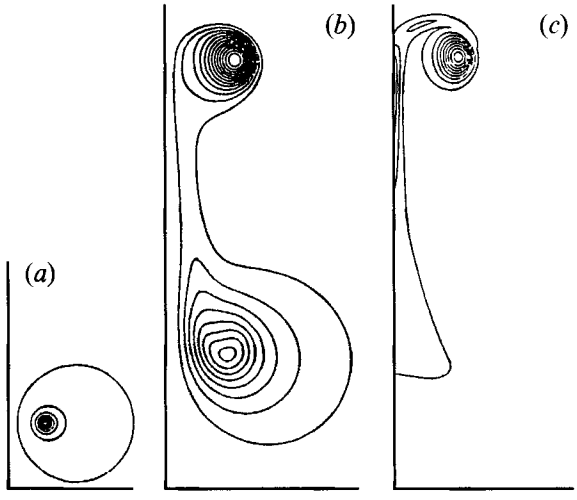

FIGURE 11. (*a*) Initial ξ-contours for case III; (*b*) ξ-contours at a late stage in the evolution; (*c*) plot of the total vorticity magnitude at the time as (*b*).

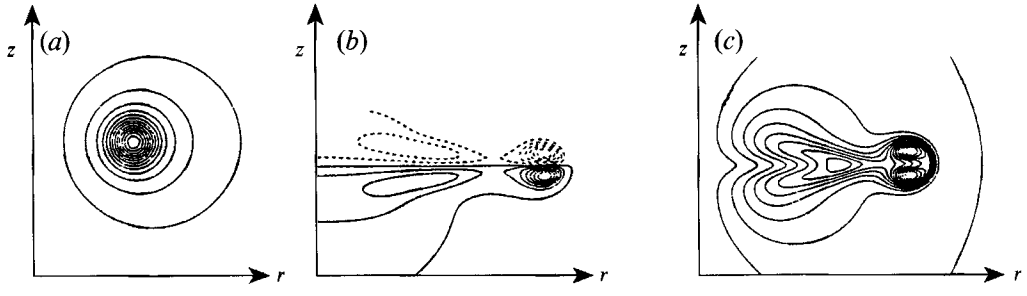

FIGURE 12. (*a*) Initial ξ-contours for case IV; (*b*) η-contours at a late stage in the evolution; (*c*) ξ-contours at the time as (*b*).

commonly used in the literature (e.g. Boratav, Pelz & Zabusky 1992), because vortex surfaces are extremely difficult to compute and bundles of vortex lines appear too messy. Thus the topology of the vorticity field must be approached with extreme care in all but the very simplest flows.

Case IV: Topology changes constrained by additional symmetry. The initial condition for this flow simulation is a jet which has been bent into a circle around the z-axis. That is, the initial condition consists of pure swirl ($\omega_\theta \equiv 0$) with a ξ-distribution as shown in figure 12(*a*). Although there is no initial azimuthal vorticity, it is quickly generate by the coupling term in the evolution equation for η, (10). The generated azimuthal vorticity forms a vortex dipole which shoots radially outward (figure 12*b*). In the process, the ξ-distribution is partly carried along; but meanwhile it deforms strongly, and steep ξ-gradients develop in various places (figure 12*c*), giving rise to significant diffusion. This type of flow has been simulated for the Euler equations by Grauer & Sideris (1991) and Siggia & Pumir (1992) with the aim of finding a finite-time singularity. Virk *et al.* (1994) simulated the flow for the Navier–Stokes equations at $Re = 800$ as an example of spatial segregation of left and right polarized vorticity. We study the topology of the vorticity field in the latter simulation here.

Initially there is only one island ($\mathfrak{I}_A$) corresponding to a single critical point A; see figure 12(*a*). Later (figures 12*c* and 13*c*), there are five critical points: three centres

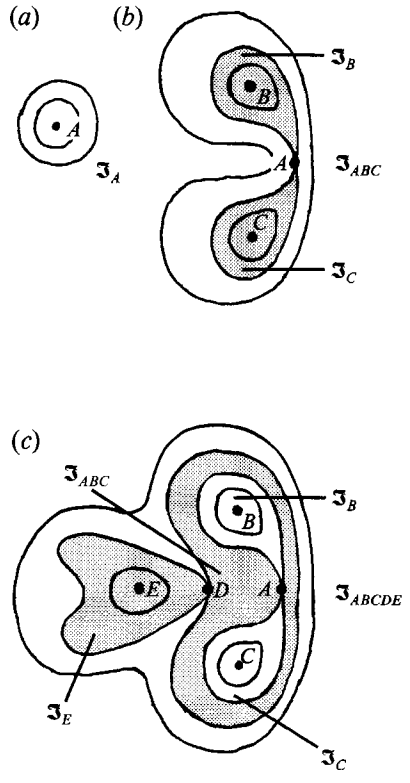

FIGURE 13. Schematic of the island structure during the evolution of case IV: (*a*) initial; (*b*) after the first bifurcation; (*c*) after the second bifurcation.

(*B*, *C* and *E*) and two saddles (*A* and *D*). (Note that *A* and *D* are not simple saddles of the type discussed in §6, but saddles with first or higher order of tangency.) Correspondingly, there are five islands: $\mathfrak{I}_B$, $\mathfrak{I}_C$, $\mathfrak{I}_{ABC}$, $\mathfrak{I}_E$ and $\mathfrak{I}_{ABCDE}$. This configuration results from two bifurcations. The first splits the original centre *A* into a saddle (*A*) and two centres (*B* and *C*); see figure 13*b*. After this bifurcation, the two centres gradually move away from the line of symmetry. The second bifurcation creates *D* and *E* on the line of symmetry, but away from *A* (figure 13*c*). Of these two topology changes only the second is catastrophic.

The symmetry (figures 12*a–c*) has some interesting implications. The fact that ξ is even in z and ω_θ is odd in z implies that vortex lines intersecting $z = 0$ (the symmetry plane) are closed with winding number $W = \infty$; see figure 14. (Note that the vortex lines are not circular, except at $t = 0$.) Consequently, all vortex lines in $\mathfrak{I}_{ABC}$, $\mathfrak{I}_E$, and $\mathfrak{I}_{ABCDE}$ are closed with infinite winding number; see figure 14(*c*). This is also true for all vortex lines in the original island $\mathfrak{I}_A$ (figure 14*a*). Moreover, *A*, *D* and *E* correspond to circles of nulls of the full three-dimensional vorticity field, for $\omega_\theta = 0$ on the symmetry plane. In the other two islands ($\mathfrak{I}_B$ and $\mathfrak{I}_C$), the vortex lines are not constrained by the symmetry, and hence obey the generic axisymmetric scenario described in §4, namely that W varies continuously across nested axisymmetric vortex surfaces. This observation makes the first bifurcation, which generates $\mathfrak{I}_B$ and $\mathfrak{I}_C$, very interesting. Before this bifurcation the vorticity field consists of vortex lines which are all unknotted, that is, no two lines are linked (figure 14*a*). After the first bifurcation, however, the lines are all knotted (figure 14*b*): the lines in $\mathfrak{I}_{ABC}$ link with all lines in

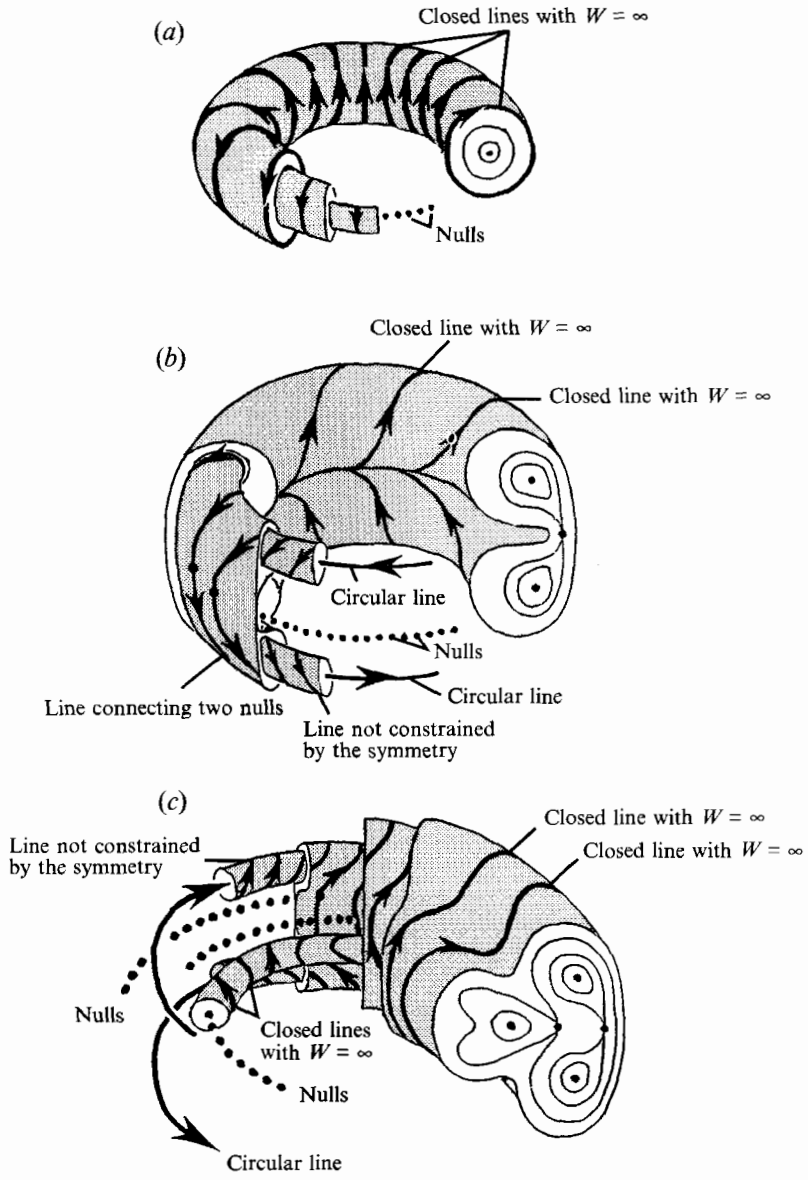

FIGURE 14. Schematic of the vortex line topology in case IV: (*a*) initial, all lines closed and unlinked; (*b*) after the first bifurcation, all lines link with other; (*c*) after the second bifurcation, some lines, namely those in island E (see figure 13*c*), are unlinked from all other lines.

$\mathfrak{I}_B$ and $\mathfrak{I}_C$; the lines in $\mathfrak{I}_B$ link with the circular line B; and the lines in $\mathfrak{I}_C$ link with the circular line C. After the second bifurcation, some vortex lines are again unknotted, namely those in island $\mathfrak{I}_E$ (figure 14*c*). Although such a collection of closed vortex lines is structurally unstable (e.g. add a small positive ω_0 component in the support of ξ and lines will no longer be closed), the present flow simulation is a prime example of how vortex lines can link and unlink in a viscous flow.

8. Discussion and conclusions

In this paper we have examined a vortex reconnection different from that previously studied. The present reconnection takes place along a closed vortex line, whereas the literature deals with reconnection at nulls of the three-dimensional vorticity field. We have examined the reconnection in the idealized setting of axisymmetric viscous flows with all three vorticity components. By insisting on structural stability with respect to axisymmetric perturbations, we have shown that the reconnection must necessarily be studied in terms of axisymmetric vortex surfaces rather than vortex lines.

Viscous axisymmetric vortex dynamics is viewed as a global bifurcation problem for the phase portrait of a dynamical system. The dynamical system is Hamiltonian with the azimuthal circulation ξ as the Hamiltonian, the meridional plane being the phase plane, the vector lines of the meridional vorticity field (the meridional cross-sections of the axisymmetric vortex surfaces) representing the phase plane trajectories, and with time as the bifurcation parameter. The variation of the Hamiltonian with the bifurcation parameter is extremely complicated, for it is governed by the partial differential equations of the fluid flow.

By recasting the viscous axisymmetric vortex dynamics in terms of a global bifurcation problem for a Hamiltonian system, we have given the concept of reconnection in axisymmetric flows a precise meaning in terms of circulation (flux) transfer between structurally stable topological entities (islands in MHD-parlance) in the phase plane. Moreover, we have given precise meanings to the concepts of circulation annihilation, and spontaneous and catastrophic topology changes of axisymmetric vortex surfaces. The dynamical system approach allows us to identify exactly the occurrence and location of reconnection, annihilation, etc. Quantitative measures associated with these concepts have also been introduced, viz. rate of reconnection R_{rec} and rate of annihilation R_a.

The dynamical system approach provides a self-consistent, physically meaningful, and simple way of tracking individual axisymmetric vortex surfaces in time, even though the flow is viscous. We have shown that this time history is equivalent to the advection of the surfaces by a uniquely defined (divergent) virtual velocity field. This velocity field is easy to calculate, but has singularities in the meridional plane. The motion of the axisymmetric vortex surfaces is frozen in the virtual velocity field except where it is singular. It is at the exact locations of these singularities that reconnection and annihilation take place. By means of a local analysis of the singularities in the virtual velocity, we show that it results in the correct rates of reconnection and annihilation (the correct rates are obvious through the dynamical system approach). Hence, the qualitative cut-and-connect procedure shown in figure 1, and prevalent in the literature, becomes correct and quantitative in terms of the virtual velocity field. The global changes in the axisymmetric vortex surface topology are also directly related to the virtual velocity field, namely through the appearance and disappearance of singularities in this velocity.

The applicability of this theoretical framework to well-resolved computationally determined flow fields has been demonstrated by four examples. Occurrence of all of the theoretically discussed phenomena (reconnection, annihilation, reconnection reversal, spontaneous topology changes, and catastrophic topology changes) have been identified in these computed flows. Except for the usual requirement of well-resolved flow fields, there are no computational difficulties in applying our concepts to axisymmetric flows.

At this point, it is appropriate to mention that Kida & Takaoka (1991) have

introduced a quantity D which they call the 'degree of vortex reconnection'. D is defined as $D = \nu\boldsymbol{\omega} \cdot \Delta\boldsymbol{\omega}$. They argue that reconnection occurs where $|D|$ is large. Note that $D = 0$ is a necessary and sufficient condition for vortex lines to be material lines (Truesdell 1954). Further, the authors claim that D must be non-zero where reconnection occurs. This is obviously not true for reconnections occurring at a vorticity null. Our case IV serves as an unusual but clear counter example. There are a number of other problems with Kida & Takaoka's argument. For example, $D \neq 0$ means slippage of vortex lines, but it has no bearing on the topology of vortex lines. Vortex lines slip (i.e. the virtual velocity differs from the fluid velocity) almost everywhere, while reconnection occurs only at certain locations. Moreover, their claim that large D locates reconnection is difficult to accept. Thus, D does not identify where reconnection occurs, does not indicate whether reconnection actually occurs, and does not quantify the process. Our obvious conclusion is that D is irrelevant for vortex reconnection.

A final comment about the extensive recent numerical attempts (e.g. Pumir & Siggia 1992; Kerr 1992; Caflisch *et al.* 1992) to locate a finite-time singularity in the three-dimensional Euler equations or even the Navier–Stokes equations at high Reynolds numbers is in order. It is a delicate and very difficult task to provide convincing numerical evidence for such a singularity, for there is usually plenty of room for doubt due to a variety of sources of numerical errors. Since vortex reconnection problems in the limit of infinite Reynolds number seem to be the prime singularity candidate (e.g. see the above references) we suggest that the numerics should be validated in flows where there is no singularity in either the infinite Reynolds number limit or in the corresponding Euler flow. Although the present paper does not in any way address the singularity issue, it does naturally suggest a class of test problems without singularities. Namely, consider a flow described by equations (4)–(6). In this two-dimensional flow, reconnection can occur for the in-plane vorticity (ω_x, ω_y) in a similar fashion as for the meridional vorticity in axisymmetric flows with swirl. However, for a two-dimensional flow as represented by (4)–(6) there is a strong and well known analytical result. Namely, if ω_z and w are initially C^∞ functions of x and y, and appropriate boundary conditions are given in the limit $x^2+y^2 \to \infty$, then ω_z and w remain C^∞ functions for all time. The in-plane vorticity, given by (4), is therefore also C^∞ for all times. This result is valid for all values of $\nu \geqslant 0$. Thus, for this type of reconnection problem, there is no finite-time singularity. Interestingly, a referee informed us that plasma physicists have long appreciated that reconnection does not imply a singularity; see Furth (1985).

We are grateful to Dr D. Virk for his assistance. This work is funded by the Air Force Office of Scientific Research under grant F496620-92-J-0200.

Appendix. Initial conditions

All simulations are performed using the axisymmetric spectral code of Virk *et al.* (1994). This algorithm allows a vorticity field $\boldsymbol{\omega}$ to be decomposed into its left- ($\boldsymbol{\omega}_L$) and right-hand components ($\boldsymbol{\omega}_R$) ($\boldsymbol{\omega}_R$ is a linear combination of eigenfunctions of the curl operator corresponding to positive eigenvalues; $\boldsymbol{\omega}_L$ is a superposition of eigenmodes corresponding to negative eigenvalues). In this way a partially polarized vorticity is constructed as $\boldsymbol{\omega}_R + (1-\chi)\boldsymbol{\omega}_L$, where the constant χ is the polarization parameter. The code uses N Bessel functions in the radial direction and M Fourier modes in the axial

direction. The computational domain has radial extent L and axial extent H. The unpolarized vortex rings from which the initial conditions are constructed all have the following profile for the azimuthal vorticity:

$$\omega_0 \exp(-4x/(1-x^2)) \exp(4x^4+4x^6+4x^8), \quad 0 < x < 1. \tag{A 1}$$

The parameters describing the initial conditions are: the ring radius R, the core radius σ, the axial position of the ring Z, the peak vorticity of the unpolarized ring ω_0, and the polarization parameter χ. We have:

Case I: $N = 100$, $M = 128$, $L = 8$, $H = 8$, $Re = 800$,
$\sigma_1 = \sigma_2 = 0.2$, $R_1 = R_2 = 2.0$, $Z_2 - Z_1 = 0.8$, $\omega_{01} = \omega_{02} = 27$, $\chi = 0.8$.

Case II: $N = 100$, $M = 192$, $L = 20$, $H = 30$, $Re = 500$,
$\sigma_1 = \sigma_2 = 0.4$, $R_1 = 3$, $R_2 = 7$, $Z_2 - Z_1 = 0$, $\omega_{01} = \omega_{02} = 3$, $\chi = 1$;
the ξ-distribution has profile (A 1) in an ellipse with $a = 3$, $b = 1.5$, $R_e = 5$ and $\xi_0 = 2\pi \times 0.63$.

Case III: $N = 100$, $M = 192$, $L = 20$, $H = 30$, $Re = 800$, $\sigma = 0.4$, $R = 2.0$, $\omega = 20$, $\chi = 0.5$.

Case IV: as case III except that $\chi = -1$.

REFERENCES

ASHURST, W. T. & MEIRON, D. I. 1987 Numerical study of vortex reconnection. *Phys. Rev. Lett.* **58**, 1632.

BORATAV, O. N., PELZ, R. B. & ZABUSKY, N. J. 1992 Reconnection in orthogonally interacting vortex tubes: Direct numerical simulations and quantifications. *Phys. Fluids* A **4**, 581–606.

CAFLISCH, R., LI, X. & SHELLEY, M. 1992 The collapse of an axisymmetric, swirling vortex sheet. *Nonlinearity* (submitted).

FOHL, F. & TURNER, J. S. 1975 Colliding vortex rings. *Phys. Fluids* **18**, 433.

FURTH, H. P. 1985 Nonideal magnetohydrodynamic instabilities and toroidal magnetic confinement. *Phys. Fluids* **28**, 1595–1611.

GRAUER, R. & SIDERIS, T. C. 1991 Numerical computation of 3D incompressible ideal fluids with swirl. *Phys. Rev. Lett.* **67**, 3511.

GREENE, J. M. 1988 Geometrical properties of three-dimensional reconnecting magnetic fields with nulls. *J. Geophys. Res.* **93**, 8583.

GREENE, J. M. 1990 Vortex nulls and magnetic nulls. In *Topological Fluid Mechanics* (ed. H. K. Moffatt & A. Tsinober), pp. 478–484. Cambridge University Press.

HUSSAIN, F. 1986 Coherent structures and turbulence. *J. Fluid Mech.* **173**, 303.

KERR, R. M. 1992 Evidence for a singularity of the three-dimensional incompressible Euler equations. In *Topological Aspects of the Dynamics of Fluids and Plasma* (ed. H. K. Moffatt, G. M. Zaslavsky, P. Comte *et al.*), pp. 309–401. Kluwer.

KERR, R. & HUSSAIN, F. 1989 Simulation of vortex reconnection. *Physica* D **37**, 474.

KIDA, S. & TAKAOKA, M. 1991 Breakdown of frozen motion of vorticity field and vorticity reconnection. *J. Phys. Soc. Japan* **60**, 2184.

MELANDER, M. V. & HUSSAIN, F. 1991 Reconnection of two antiparallel vortex tubes: A new cascade mechanism. In *Turbulent Shear Flows 7* (ed. F. Durst *et al.*). Springer.

MOFFATT, H. K. & TSINOBER, A. (ed.) 1990 *Topological Fluid Mechanics*. Cambridge University Press.

MOFFATT, H. K., ZASLAVSKY, G. M., COMTE, P. & TABOR, M. (ed.) 1992 *Topological Aspects of the Dynamics of Fluids and Plasmas*. Kluwer.

NEWCOMB, W. A. 1958 Motion of magnetic lines of force. *Ann. Phys. N.Y.* **3**, 347.

OSHIMA, Y. & IZUTZU, N. 1988 Cross-linking of two vortex rings. *Phys. Fluids* **31**, 2401.

PUMIR, A. & SIGGIA, E. D. 1992 Development of singular solutions to the axisymmetric Euler equations. *Phys. Fluids* A **4**, 1472.

SCHATZLE, P. 1987 An experimental study of fusion of vortex rings. PhD thesis, Graduate Aeronautical Laboratories, Calif. Inst. Tech.

SCHWARZ, K. 1985 Three-dimensional vortex dynamics in superfluid ^{4}He line-line and line-boundary interaction. *Phys. Rev.* B **31**, 5782.

SHELLEY, M. J., MEIRON, D. I. & ORSZAG, S. A. 1993 Dynamical aspects of vortex reconnection of perturbed anti-parallel vortex tubes. *J. Fluid Mech.* **246**, 613.

TRUESDELL, C. 1954 *The Kinematics of Vorticity*. Indiana University Publ., Science series No. 19.

VIRK, D., MELANDER, M. V. & HUSSAIN, F. 1994 Dynamics of a polarized vortex ring. *J. Fluid Mech.* **260**, 23–55.

WINKELMANS, G. & LEONARD, A. 1989 Improved vortex methods for three-dimensional flows. In *Mathematical Aspects of Vortex Dynamics* (ed. R. E. Calflish), pp. 25–35. SIAM.

ZABUSKY, N. J. & MELANDER, M. V. 1989 Three-dimensional vortex tube reconnection: morphology for orthogonally-offset tubes. *Physica* D **37**, 555.